Amplitude tuning of steady-state entanglement in strongly driven coupled qubits

Ana Laura Gramajo, Daniel Domínguez, and María José Sánchez
Centro Atómico Bariloche and Instituto Balseiro, 8400 San Carlos de Bariloche, Argentina

(Received 29 June 2018; published 30 October 2018)

We report a mechanism to generate dissipative steady-state entanglement in coupled solid-state qubits driven by strong periodic fields. We demonstrate that steady entanglement can be induced and tuned by changing the amplitude of the driving field. A rich dynamic behavior with *creation, death, and revival* of entanglement can be observed near multiphoton resonances. Coupled superconducting qubits are good candidates for the observation of these effects.

DOI: 10.1103/PhysRevA.98.042337

I. INTRODUCTION

The generation and stabilization of entanglement is one of the main challenges in quantum information applications. In recent years, strategies based on the creation of steady-state entanglement through engineered dissipation have been discussed theoretically [1–4] and demonstrated in experiments [5–11]. In this scheme, the system of interest is driven by external fields and coupled to a reservoir, developing a nontrivial nonequilibrium dynamics that leads to a highly entangled steady state. The effective relaxation rates can be tuned by adequately designing the quantum reservoir, the system-reservoir couplings, or the driving protocols. Experimental demonstrations include realizations with trapped ions [5–7], atomic ensembles [8], and superconducting qubits [9–13]. Another strategy for entanglement stabilization is measurement-based protocols, which have been implemented, for example, in coupled superconducting qubits [14–18].

The different proposed mechanisms for driven dissipative entanglement generation utilize *weak* resonant drivings to tailor the relaxation processes [1–3,5–13]. In contrast to the weak resonant driving protocols, suitable to quantum optics studies aimed to manipulate atoms with light, for *large*-amplitude periodic drivings interesting nonperturbative effects are known to exist. Among these, coherent destruction of tunneling [19–21], Landau-Zener-Stückelberg (LZS) interferometry [22–31], and bath-mediated population inversion [32–35] have been studied in two-level systems built from superconducting devices and quantum dots.

In the case of superconducting devices driven by an external (dc+ac) magnetic field, the LZS amplitude spectroscopy has become a tool to access the multilevel structure of these artificial atoms, beyond the two lowest-energy levels that define the qubit [22].

On the theoretical side, the Floquet formalism [36] has been employed to solve the dynamics of strongly driven single qubits in terms of quasienergies and Floquet states [37–39]. This nonperturbative formalism goes beyond the rotating-wave approximation, usually employed for the weak driving regime, which breaks down for strong driving amplitudes.

Quite exceptional are the studies of entanglement generation in the framework of Floquet theory. Reference [40] focused on the case of two weakly coupled qubits, and Ref. [41] extended the study for arbitrary couplings and large ac driving amplitudes. However, these researches were restricted to the highly coherent regime, i.e., when the driving is on for timescales shorter than the decoherence time.

In this work we present a mechanism to induce steady-state entanglement by means of large-amplitude periodic drivings. Using as a test system two coupled qubits, we will demonstrate that the entanglement in the steady state can be induced and tuned by changing the amplitude of a driving periodic field. One of our main results is advanced in Fig. 1(a) where we show how the concurrence (a measure of entanglement) can be increased or decreased as a function of the amplitude of the periodic driving.

II. MODEL AND DEFINITIONS

In this work we consider two coupled qubits with Hamiltonian $\hat{H}_s(t) = \hat{H}_0 + \hat{V}(t)$, where

$$\hat{H}_0 = \sum_{i=1}^{2}\left(-\frac{\epsilon_0}{2}\sigma_z^{(i)} - \frac{\Delta_i}{2}\sigma_x^{(i)}\right) - \frac{J}{2}\left(\sigma_+^{(1)}\sigma_-^{(2)} + \sigma_-^{(1)}\sigma_+^{(2)}\right) \tag{1}$$

with $\sigma_{z,x,+,-}^{(i)}$ the Pauli matrices in the Hilbert space of qubit i [42]. This type of Hamiltonian can be realized, for instance, in superconducting qubits [43–48], where Δ_1, Δ_2, J are fixed device parameters and ϵ_0 can be controlled experimentally. In the case of flux qubits, ϵ_0 can be controlled by an external magnetic flux through each qubit device, the Δ_1, Δ_2 are determined by the relation among the charging energy and the Josephson energy of the junctions in the circuit, and the qubit-qubit coupling can been achieved in different ways in the laboratory (inductive couplings, capacitive couplings, or mediated through a cavity) [42–48]. The external ac driving field is $\hat{V}(t) = -A\cos(\omega t)(\sigma_z^{(1)} + \sigma_z^{(2)})/2$, of amplitude A and frequency ω [40,41,49–52]. In the case of flux qubits, $\hat{V}(t)$ corresponds to applying a time-periodic magnetic flux in each qubit, with frequencies that are typically in the microwave range.

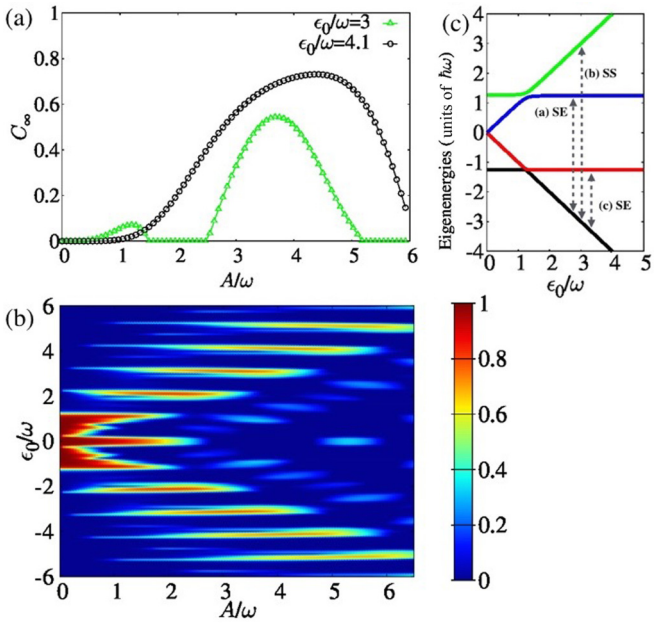

FIG. 1. (a) Plots of the steady-state concurrence C_∞ as function of the driving amplitude A/ω for $\epsilon_0/\omega = 3$ (green triangles) and $\epsilon_0/\omega = 4.1$ (black circles). (b) Intensity plot of C_∞ versus A/ω and ϵ_0/ω. (c) Eigenenergies E_i of the system Hamiltonian H_0 as a function of ϵ_0/ω. Along this work, we choose $\Delta_2/\Delta_1 = 1.5$, $J/\Delta_1 = -25$, and $\omega/\Delta_1 = 10$. The bath temperature is taken as $T_b/\Delta_1 = 0.0467$ and for the bath spectral density we consider $\gamma = 0.001$ with a cutoff frequency $\omega_c/\Delta_1 = 333$. See text for details.

Dissipation and decoherence are taken into account by considering the open-system dynamics, with global Hamiltonian

$$\hat{\mathcal{H}}(t) = \hat{H}_s(t) + \hat{H}_b + \hat{H}_{sb}.$$

Since $\hat{H}_s(t) = \hat{H}_s(t+T)$ with $T = 2\pi/\omega$ the driving period, it is convenient to use the Floquet formalism, that allows to treat periodic forces of arbitrary strength and frequency [36–39]. In the Floquet formalism, the solutions of the time-dependent Schrödinger equation are of the form $|\Psi_\alpha(t)\rangle = e^{i\gamma_\alpha t/\hbar}|\alpha(t)\rangle$, where the Floquet states $|\alpha(t)\rangle$ satisfy $|\alpha(t)\rangle = |\alpha(t+T)\rangle = \sum_K |\alpha(K)\rangle e^{-iK\omega t}$, and are eigenstates of the equation $[\mathcal{H}(t) - i\hbar\partial/\partial t]|\alpha(t)\rangle = \gamma_\alpha|\alpha(t)\rangle$, with γ_α the associated quasienergy.

We consider a thermal bath at temperature T_b described by the usual harmonic oscillators Hamiltonian $\hat{H}_b$. The bath is linearly coupled to the two-qubits system in the form $\hat{H}_{sb} = g\mathcal{A}\otimes\mathcal{B}$, with g the coupling strength, $\mathcal{B}$ an observable of the bath, and $\mathcal{A}$ the observable of the system. Here, we consider $\mathcal{A} = \sigma_z^{(1)} + \sigma_z^{(2)}$, that corresponds to flux noise in the case of flux qubits, and to charge noise in the case of charge qubits, which in both cases is the dominant mechanism of coupling to the environment.

The bath degrees of freedom are characterized by the Ohmic spectral density $J(\Omega) = \gamma\Omega e^{-|\Omega|/\omega_c}$, with ω_c the cutoff frequency and $\gamma \propto g^2$. The Von Neumann equation for the time evolution of the reduced density matrix $\rho(t) = Tr_b(\rho_{\rm tot}(t))$ is

$$\dot{\rho}(t) = -\frac{i}{\hbar}Tr_b([\hat{\mathcal{H}}(t), \rho_{\rm tot}(t)]). \tag{2}$$

After expanding $\rho(t)$ in terms of the time-periodic Floquet basis $\{|\alpha(t)\rangle\}$ ($\alpha, \beta = 0, 1, 2, 3$)

$$\rho_{\alpha\beta}(t) = \langle\alpha(t)|\rho(t)|\beta(t)\rangle, \tag{3}$$

the Born (weak coupling) and Markov (fast relaxation) approximations for the time evolution are performed. It is further assumed that at time $t = 0$ the bath is in thermal equilibrium and uncorrelated with the system. We note here that there is a subtlety concerning different procedures of performing the Markovian approximation. In general, the Markovian approximation for the eigenenergy spectrum performed on the level of the undriven Hamiltonian differs from performing it on the level of the driven Floquet quasienergy spectrum [53,54]. This latter approach, that leads to the Floquet-Markov master equation, is more appropriate for strongly driven solid-state qubits since it is valid for arbitrary large driving strengths [53–55].

Following this procedure, the resulting Floquet-Markov master equation [37,38,53–57] is

$$\dot{\rho}_{\alpha\beta}(t) = -i(\gamma_\alpha - \gamma_\beta)\rho_{\alpha\beta} - \sum_{\alpha'\beta'}\mathcal{L}_{\alpha\beta,\alpha'\beta'}(t)\rho(t)_{\alpha'\beta'}. \tag{4}$$

Considering that the timescale t_r for full relaxation satisfies $t_r \gg T$, the transition rates $\mathcal{L}_{\alpha\beta,\alpha'\beta'}(t)$ can be approximated by their average over one period T [53,54], obtaining

$$\begin{aligned}\overline{\mathcal{L}_{\alpha\beta,\alpha'\beta'}(t)} &= L_{\alpha\beta,\alpha'\beta'} \\ &= \delta_{\beta\beta'}\sum_\eta R_{\eta\eta,\alpha'\alpha} + \delta_{\alpha\alpha'}\sum_\eta (R_{\eta\eta,\beta'\beta})^* \\ &\quad - R_{\alpha\beta,\alpha'\beta'} - (R_{\beta\alpha,\beta'\alpha'})^*,\end{aligned} \tag{5}$$

where the rates

$$R_{\alpha\beta,\alpha'\beta'} = \sum_Q g^Q_{\alpha\alpha'}A^Q_{\alpha\alpha'}\left(A^Q_{\beta\beta'}\right)^* \tag{6}$$

can be interpreted as sums of Q-photon exchange terms, with $g^K_{\alpha\beta} = J(\gamma_{\alpha\beta} + K\omega)n_{th}(\gamma_{\alpha\beta} + K\omega)$, and $\gamma_{\alpha\beta} = \gamma_\alpha - \gamma_\beta$ and $K \in \mathbb{Z}$. The thermal occupation is given by the Bose-Einstein function $n_{th}(x) = 1/(e^{x/k_BT} - 1)$.

Each $A^K_{\alpha\beta}$ is a transition matrix element in the Floquet basis, defined as

$$A^K_{\alpha\beta} = \sum_L \langle\alpha(L)|\mathcal{A}|\beta(L+K)\rangle, \tag{7}$$

with $|\alpha(L)\rangle$ the $L \in \mathbb{Z}$ Fourier component of the Floquet state.

We obtain numerically the Floquet components $|\alpha(K)\rangle$ and then we calculate the rates $R_{\alpha\beta\alpha'\beta'}$ and $L_{\alpha\beta\alpha'\beta'}$. Once the $L_{\alpha\beta\alpha'\beta'}$ terms are obtained, the time-dependent solution of $\rho_{\alpha\beta}(t)$ and the steady state $\rho_{\alpha\beta}(t\to\infty)$ are computed as described in Ref. [35]. We calculate numerically the steady state $\rho(t\to\infty)$ and the time dependent $\rho(t)$ taking as initial condition the ground state of $\hat{H}_0$. We will consider in the numerical simulations device parameters ϵ_0, Δ_1, Δ_2, J, dissipation strength γ, bath temperature T_b, driving frequency ω, and amplitudes A within the ranges available in solid-state qubits [43–48].

We choose as an entanglement measure the concurrence, which can be calculated for mixed states as $C = \max\{0, \lambda_4 - \lambda_3 - \lambda_2 - \lambda_1\}$, where λ_i's are real numbers in decreasing

order and correspond to the eigenvalues of the matrix $R = \sqrt{\sqrt{\rho}\tilde{\rho}\sqrt{\rho}}$, with $\tilde{\rho} = \sigma_y^{(1)} \otimes \sigma_y^{(2)} \rho^* \sigma_y^{(1)} \otimes \sigma_y^{(2)}$ [58]. The concurrence can be accessed experimentally in solid-state qubits through quantum tomography measurements [16].

III. AMPLITUDE TUNING OF STEADY ENTANGLEMENT: NUMERICAL RESULTS

From the results presented along this work, it follows that the relevant entanglement dynamics takes place near the resonance conditions. The manipulation of entanglement by an ac drive has been already studied in closed systems, neglecting the effect of the thermal bath. For two isolated coupled qubits, the generation of entanglement can occur at and near n-photon resonances [40,41]. We will investigate here the effect of noise and dissipation in the entanglement generation by solving numerically the open-system dynamics.

The system Hamiltonian H_0, for $\Delta_1, \Delta_2 \ll \epsilon_0$, has two entangled eigenstates with their corresponding eigenenergies:

$$\begin{aligned} |e_+\rangle &\approx \frac{1}{\sqrt{2}}(|01\rangle + |10\rangle), \quad E_{e+} \approx -J/2, \\ |e_-\rangle &\approx \frac{1}{\sqrt{2}}(|01\rangle - |10\rangle), \quad E_{e-} \approx +J/2 \end{aligned} \tag{8}$$

(in the basis spanned by the eigenstates of $\sigma_z^{(1)} \otimes \sigma_z^{(2)}$), and two separable (disentangled) eigenstates

$$\begin{aligned} |s_0\rangle &\approx |00\rangle, \quad E_{s0} \approx -\epsilon_0, \\ |s_1\rangle &\approx |11\rangle, \quad E_{s1} \approx +\epsilon_0. \end{aligned} \tag{9}$$

The ground state is entangled ($|E_0\rangle \approx |e_-\rangle$) with concurrence $C \approx 1$ for $|\epsilon_0| < |J|/2$ and separable ($|E_0\rangle \approx |s_0\rangle$) for $|\epsilon_0| > |J|/2$, with $C \approx 0$. In Fig. 1(c) we plot the eigenenergies E_i as a function of ϵ_0 for $J = -25\Delta_1$.

We calculate the resonance conditions considering the Hamiltonian $H_s(t) = \hat{H}_0 + \hat{V}(t)$, as it was already done in Ref. [38]. In the Floquet approach, the resonance conditions correspond to $\gamma_\alpha - \gamma_\beta = m\omega$. The quasienergies, computed for $\Delta_i/\omega \to 0$ using perturbation theory [39] in the lowest order, are $\gamma_\alpha \sim \pm\epsilon_0 + n\omega$ and $\pm J/2 + n\omega$ with $n \in \mathbb{Z}$, which correspond to separable and entangled states, respectively. As for $\Delta_i/\omega \to 0$, the driving $\hat{V}(t)$ and the coupling Hamiltonian commute, the location of the avoided (quasi)crossings in the spectrum of quasienergies are replicas (in $\pm n\omega$) of the quasicrossings of the static spectrum. The resonance conditions $\gamma_\alpha - \gamma_\beta = m\omega$, $m \in \mathbb{Z}$, in the lowest order in Δ_i/ω coincide with the condition $E_i - E_j \approx m\omega$. We classify the resonances according to the involved states: the SS resonance (separable-separable states), SE resonance (separable-entangled states and vice versa), and EE resonance (entangled-entangled states). The corresponding resonance conditions are

$$\begin{aligned} 2\epsilon_0 &\sim m\omega, \quad \text{SS resonances} \\ \epsilon_0 \pm J/2 &\sim m\omega, \quad \text{SE resonances} \\ J &\sim m\omega, \quad \text{EE resonances} \end{aligned} \tag{10}$$

with $m \in \mathbb{Z}$. In Fig. 1(c) we show the energy spectrum of H_0 as a function of ϵ_0, and the location of some resonances are plotted with dashed black lines, allowing to identify each resonance condition.

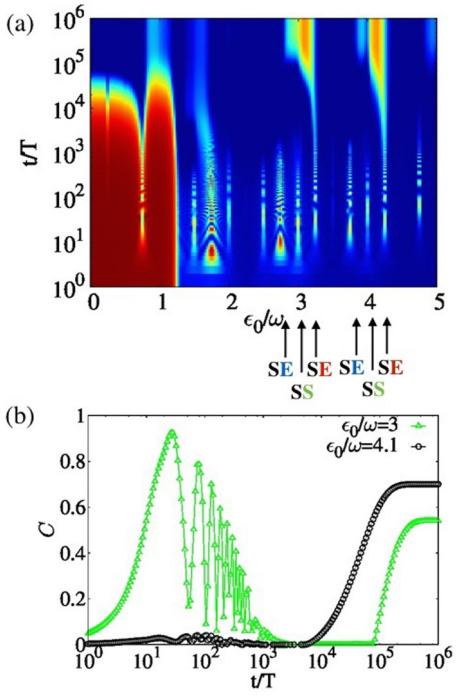

FIG. 2. (a) Intensity plot of C versus ϵ_0/ω and t/T. The location of some of the SE (SS) resonances are indicated. (b) Plot of C as a function of the time t/T for $\epsilon_0/\omega = 3$ (green triangles) and $\epsilon_0/\omega = 4.1$ (black circles). The initial condition corresponds to the ground state for the correspondent ϵ_0/ω. The results correspond to $A/\omega = 3.8$. Other parameters are the same as in Fig. 1.

Let us analyze what happens for the open-system situation considered in this work. From now on, we will focus on the possibility of entanglement generation when the ground state is separable, $|\epsilon_0| > |J|/2$. Figure 1(b) shows the concurrence C_∞ in the stationary regime, as a function of A and ϵ_0, for $J/\Delta_1 = -25$. When the driving is on, $A \neq 0$, we find that entanglement generation takes place for certain values of ϵ_0, which are close to the SE resonances at $\epsilon_0 \approx |J|/2 + n\omega$. As it is shown in detail in Fig. 1(a), in these cases the concurrence is modulated by the driving amplitude and, by adequately tuning A, C_∞ can reach values close to 1, corresponding to a maximally entangled Bell's state, even when the ground state is separable.

To understand why there is generation of steady entanglement near SE resonances, it is necessary to analyze in detail the time evolution of the system. Figure 2(a) shows $C(t)$ as a function of ϵ_0/ω and the normalized time t/T for a fixed value of amplitude $A/\omega = 3.8$, with $T = 2\pi/\omega$. It is straightforward to observe that the concurrence displays a rich dynamics near the multiphoton resonances. At short times there is a driving-induced generation of entanglement at and near the values of ϵ_0 corresponding to SS or to SE resonances. This *short-time dynamic entanglement creation* is carried out by the coherent superposition of states induced by the driving, and corresponds to the usual Rabi-type oscillations at multiphoton resonances [27,59]. Similar results have been obtained for the isolated system, as we already mentioned [41]. In that case, the concurrence in the parameter space $[\epsilon_0, A]$ presents a pattern that can be understood in terms

of Landau-Zener-Stückelberg (LZS) interference, extensively studied and observed in single superconducting qubits [27]. However, for times above the decoherence time $t > t_c$ (with $t_c \sim 10^3 T$ in Fig. 2), we find that the driven induced entanglement fades away in the case of the SS resonances. In this situation, the entanglement is fragile against the noise of the external environment and it is easily destroyed beyond the decoherence time.

A strikingly different behavior takes place in the case of SE resonances. At large timescales, above the relaxation time $t_r > t_c$, we find the generation of steady entanglement at one side of the SE resonances. As an example, we show in Fig. 2(b) the time evolution of the concurrence for two off-resonant cases that are close to an SE resonance. For $\epsilon_0/\omega = 4.1$ (shown in black circles), that is below the SE resonance at $\epsilon_0/\omega = 4.25$, we see that at initial times the entanglement is negligible (the concurrence is very small) and only after driving the system for large times, above $t_r \sim 10^4 T$, steady entanglement is created. The entanglement induced in this latter case is robust and stable at long times, opposite to the SS resonance situation previously described. Another interesting and nontrivial behavior takes place for $\epsilon_0/\omega = 3$, which corresponds to an SS resonance that is very close to the SE resonance at $\epsilon_0/\omega = 3.25$ [this $C(t)$ is plotted with a green triangles in Fig. 2(b)]. At $t = 0$, the ground state is disentangled and $C \approx 0$. After the driving is turned on, there is a dynamic generation of entanglement due to a Rabi-type resonance among two separable states, giving place to an oscillating $C(t)$ that can reach values close to 1. At the decoherence time, this entanglement dies off and the concurrence drops to zero for $t > t_c \sim 10^3 T$, and stays at this value for times up to $10^5 T$. Above this latter time, steady-state entanglement sets in, which is induced due to the nearness to the SE resonance at $\epsilon_0/\omega = 3.25$. Thus, those cases where SS and SE resonances are close exhibit a rich behavior as a function of time with *creation, death, and revival* of entanglement.

The dynamics of the two paradigmatic examples discussed above can be better described in terms of quantum tomography by evaluating the time evolution of individual components of the density matrix. In Fig. 3 we present the plot of the density matrix elements ρ_{kl} as function of t/T using the eigenstate basis $\{|E_k\rangle\}$, with $k, l = 0, \ldots, 3$. [See Fig. 1(c), where the corresponding eigenenergies are plotted versus ϵ_0/ω.] As the off-diagonal ρ_{kl} (not shown in the plot) become negligibly small above the decoherence time, the interesting behavior is obtained for the populations, given by the diagonal terms ρ_{ii}. Figure 3(a) shows the case for $\epsilon_0/\omega = 4.1$, where the ground state (black triangles) is separable, and is close to a resonance with the first excited state (red circles), which is entangled. The population of the two other eigenstates is negligible along all the time evolution, and the dynamics can be reduced to the subspace of the two states that are near resonance. Since the system is off resonance, the population remains mostly in the ground state, which corresponds to the initial condition. At large times, above t_r, the population of the first excited state rapidly increases and the ground state is depopulated. This explains the sudden creation of entanglement shown in Fig. 2(b) for this case since the first excited state is entangled. The case of creation, death, and revival of entanglement is

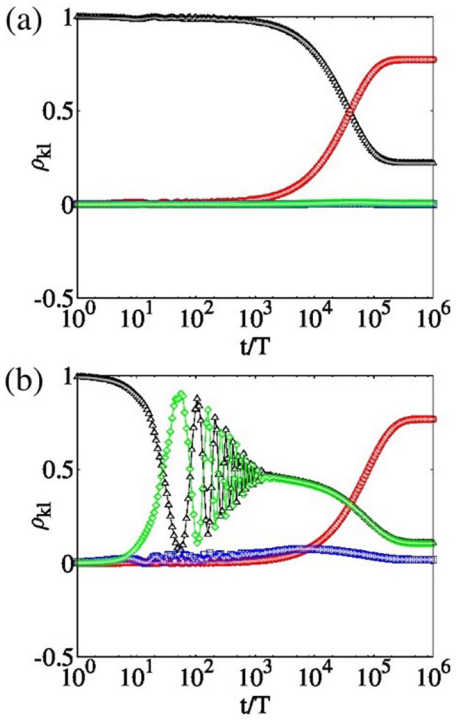

FIG. 3. Plots corresponding to the quantum tomography of two-qubits density matrix ρ as function of normalized time t/T for $A/\omega = 3.8$, and for $\epsilon_0/\omega = 4.1$ (a) and $\epsilon_0/\omega = 3$ (b). Matrix elements ρ_{kl} are in the eigenstate basis. The colors of the symbols correspond to the colors representing eigenstates in Fig. 1(c): $|s_0\rangle$, ground state (black triangles); $|e_-\rangle$, first excited state (red circles); $|e_+\rangle$, second excited state (blue squares); and $|s_1\rangle$, third excited state (green diamonds).

plotted in Fig. 3(b), for $\epsilon_0/\omega = 3$. Here, the ground state (black triangles) is at resonance with the third excited state (green diamonds), and both are separable states. For times $t < t_c$, their populations display Rabi-type oscillations while the populations of the other two states are negligible. Close to the decoherence time the oscillations are damped, and both populations tend to be equal to $\frac{1}{2}$. Above t_c the coherence between these two states is lost, and the concurrence vanishes. At larger timescales, above t_r, a rapid transfer of population to the first excited state (red circles) sets in, with almost all of the population being transferred to the entangled state.

IV. AMPLITUDE TUNING OF STEADY ENTANGLEMENT: MECHANISM

The behavior seen in Fig. 3(a) is reminiscent of the dynamic transition found in driven dissipative two-level systems near a multiphoton resonance [34,35], where population inversion can be induced in the steady state. The relaxation rate is strongly dependent on the amplitude A and, in the case of two-level systems, it has been written as a sum of terms $\Gamma_r(A) = \sum_n \Gamma_r^{(n)}(A)$ [28,35,38]. The terms in the sum correspond to driving induced photon-exchange processes with the bath, where $\Gamma_r^{(0)}$ describes the conventional relaxation process (without exchange of virtual photon) and $\Gamma_r^{(\pm n)}$ corresponds to the ac contribution due to the exchange of n virtual photon

with energy $\pm n\hbar\omega$. In this section, we estimate the rates $\Gamma_r^{(n)}$ near a multiphoton resonance showing that their dependence with the driving amplitude A is the underlying mechanism for the generation of entanglement in the steady state presented in the previous section.

The Floquet-Markov equation (4) is obtained after performing the Born and Markov approximations. A further simplification can be performed by the secular approximation where, after transforming the equation to the interaction picture, all the oscillating contributions with $e^{\pm i(\gamma_\alpha-\gamma_\beta)t}$ and $e^{\pm i(\omega-\omega')t}$ are neglected for $\alpha\neq\beta$ and $\omega\neq\omega'$ [53,55,60–62]. The resulting master equation can be written as

$$\frac{d\rho}{dt} = -i[H_s(t),\rho] + \sum_{\alpha,\beta}\Gamma_{\alpha\beta}\left\{\hat{C}_{\alpha\beta}\,\rho\,\hat{C}_{\alpha\beta}^\dagger - \frac{1}{2}\hat{C}_{\alpha\beta}^\dagger\hat{C}_{\alpha\beta}\,\rho - \frac{1}{2}\rho\,\hat{C}_{\alpha\beta}^\dagger\hat{C}_{\alpha\beta}\right\} \tag{11}$$

with the jump operators $\hat{C}_{\alpha\beta} = |\alpha(t)\rangle\langle\beta(t)|$ and the rates

$$\Gamma_{\alpha\beta} = 2R_{\alpha\alpha\beta\beta} = 2\sum_K g_{\alpha\beta}^K\left|A_{\alpha\beta}^K\right|^2. \tag{12}$$

Equation (11) is of Lindblad type since it preserves the positivity of the density operator [62]. In the Floquet basis it splits in two separate equations:

$$\frac{d\rho_{\alpha\alpha}}{dt} = \sum_\beta \Gamma_{\alpha\beta}\rho_{\beta\beta} - \Gamma_{\beta\alpha}\rho_{\alpha\alpha},$$
$$\frac{d\rho_{\alpha\beta}}{dt} = [-i(\gamma_\alpha-\gamma_\beta)-\lambda_{\alpha\beta}]\,\rho_{\alpha\beta}, \quad \alpha\neq\beta \tag{13}$$

with $\lambda_{\alpha\beta} = \sum_\eta \frac{1}{2}(\Gamma_{\alpha\eta}+\Gamma_{\eta\beta})$. For timesscales satisfying $t \gg t_c$ (with $t_c \propto \lambda_{\alpha\beta}^{-1}$ the decoherence time) the density matrix becomes diagonal in the Floquet basis [55,56,60]. The secular approximation that leads to Eq. (11) is not completely correct at the resonances [55,56], but works well off resonance and even arbitrarily close to a resonance for sufficiently small coupling to the environment [35,56].

A phenomenological explanation of the mechanism leading to an entangled steady state near the SE resonances is as follows. Near a resonance the population is concentrated in the two states intervening in the resonance. Therefore, we reduce the dynamics to the subspace of the two Floquet states $\{|a(t)\rangle, |b(t)\rangle\}$ that satisfy the resonance condition $\gamma_a-\gamma_b \approx n\omega$. We then write, for $t \gg t_c$, a Pauli-type equation for the populations of the two states near a SE resonance:

$$\frac{dP_a}{dt} = \Gamma_{ab}P_b - \Gamma_{ba}P_a,$$
$$\frac{dP_b}{dt} = \Gamma_{ba}P_a - \Gamma_{ab}P_b. \tag{14}$$

For the two Floquet states $|a\rangle, |b\rangle$, the relaxation rate that follows from the above equation is $\Gamma_r = \Gamma_{ab}+\Gamma_{ba}$. Using Eq. (6), we can decompose the relaxation rate as a sum of terms that describe virtual n-photon transitions (see the Appendix and Ref. [38]):

$$\Gamma_r = \Gamma_r^{(0)} + \sum_{n\neq 0}\Gamma_r^{(n)} \tag{15}$$

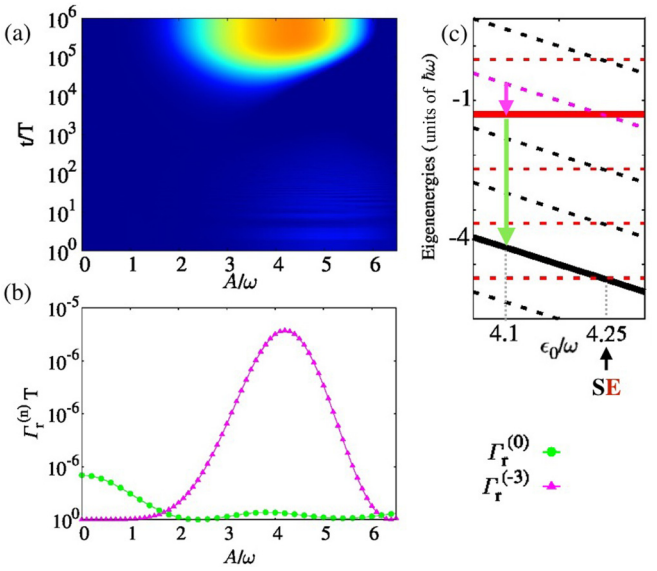

FIG. 4. (a) Intensity plot of $C(t)$ as a function of A/ω and t/T. (b) Terms $\Gamma_r^{(n)}$ that contribute to the relaxation rate are plotted as a function of the driving amplitude A/ω. Both cases correspond to $\epsilon_0/\omega = 4.1$. (c) Schematic representation of the involved transition processes between the states $|E_0\rangle = |s_0\rangle$ (black line) and $|E_1\rangle = |e_-\rangle$ [red (light gray) line]. The dashed lines represent the eigenenergies plus the addition of integer multiples of $\hbar\omega$.

with

$$\Gamma_r^{(n)} = 2\left(g_{ab}^n\left|A_{ab}^n\right|^2 + g_{ba}^n\left|A_{ba}^n\right|^2\right). \tag{16}$$

The $\Gamma_r^{(0)}$ corresponds to the direct relaxation from the excited state to the ground state, and it is the dominant relaxation mechanism for low A. For large amplitudes $A \gtrsim \omega$, the rates $\Gamma_r^{(n)}(A)$ oscillate as a function of A/ω. Within a perturbative approach for $\Delta_i \ll \omega$, it can be shown that their main dependence with the amplitude A is

$$\Gamma_r^{(n)} \propto J_n^2(A/\omega),$$

with $J_n(x)$ the Bessel function of order n. (See the Appendix for the calculation.) This Bessel function dependence with A allows that for certain ranges of A the direct term $\Gamma_r^{(0)}$ vanishes, while $\Gamma_r^{(n)}$ becomes large for some n.

The dynamic transition leading to population inversion at the side of a m-photon resonance happens for the ranges of amplitude satisfying $\Gamma_r^{(-m)}(A) \gg \Gamma_r^{(0)}(A)$ [35]. In this case, the $\Gamma_r^{(-m)}$ term corresponding to the absorption of m photons from the ground state followed by a relaxation to the first excited state prevails instead of the standard relaxation from the excited state to the ground state. Thus, whenever there is population inversion, the dc relaxation terms $\Gamma_r^{(0)}$ vanish while it is expected that one of the $\Gamma_r^{(-m)}$ terms becomes dominant.

In Fig. 4(a) we plot the time dependence of the concurrence as a function of A/ω for $\epsilon_0 = 4.1$ below a $(m=3)$-photon SE resonance. Here, we see that for certain values of A there is generation of entanglement in the steady state. Figure 4(b) shows the calculated $\Gamma_r^{(0)}(A)$ and $\Gamma_r^{(-3)}(A)$ rates as a function of A/ω while Fig. 4(c) shows schematically the relaxation

processes that correspond to each case. Comparing Figs. 4(a) and 4(b) we see that steady-state entanglement corresponds to the range of A where $\Gamma_r^{(-3)}(A) \gg \Gamma_r^{(0)}(A)$. This shows that by tuning the value of A near an SE resonance, one can attain the conditions for populating the first excited state at long times, leading to the generation of stable steady-state entanglement.

V. CONCLUSIONS

The generation of driven-dissipative steady entanglement is based on specifically engineering the reservoir, the system-reservoir coupling, and the driving protocol such that the quantum jump operators and the dissipation rates of the corresponding Linblad equation lead to the desired entangled steady state [1]. In the mechanism discussed in this work, the quantum jump operators $\hat{C}_{\alpha\beta}$ and the rates $\Gamma_{\alpha\beta}$ strongly depend on the driving amplitude A. We show that by adequately sweeping A, one can tune the terms of the quantum master equation such that the steady state is entangled. The regime of large amplitudes needed for this type of tuning is accessible in the solid-state qubits where Landau-Zener-Stuckelberg interferometry has been observed [22–31].

The particular two-qubit system studied here is an example of how this amplitude-tuned steady entanglement can be generated. From the analysis of our results, we conclude that the relevant general conditions needed for generation of steady entanglement near a SE resonance are as follows: (i) a range of the control parameter (ϵ_0 in our case) where there is a separable ground state and an entangled excited state; (ii) an avoided crossing among these two states with gap Δ within the available range of the control parameter; (iii) to be able to access experimentally to the driving frequency and amplitude regime of $\Delta < \omega < A$; and (iv) a dissipative coupling to a thermal bath.

To summarize, we have found three different dynamical regimes for entanglement evolution in driven coupled qubits: (i) Below the decoherence time $t < t_c$, there is a dynamic generation of entanglement at multiphoton resonances, as described in [40,41]. (ii) For times $t_c < t < t_r$, there is a long-time interval of *entanglement blackout*, where entanglement is destroyed due to decoherence with the environment. (iii) Above the relaxation time $t > t_r$, entanglement is created and preserved for long times near the SE resonances. This latter effect enables the generation of steady-state entanglement, which can be tuned as a function of the driving amplitude A. Quantum state tomography measurements [12,16] in solid-state devices where Landau-Zener-Stückelberg interferometry has been studied in single qubits [22–31] are good candidates to test this mechanism for entanglement generation.

ACKNOWLEDGMENTS

We acknowledge financial support from CNEA, CONICET (Grant No. PIP11220150100756), UNCuyo (Grant No. P 06/C455), and ANPCyT (Grants No. PICT2014-1382 and No. PICT2016-0791).

APPENDIX: VAN VLECK NEARLY DEGENERATE APPROXIMATION: ANALYTICAL CALCULATION OF THE RELAXATION RATES

In this appendix we calculate an analytical expression for the relaxation rate Γ_r near a resonance condition. We solve the dynamic of the system using the Floquet formalism under the Van Vleck near-degenerate approach [38].

We start considering the case $\Delta_i \to 0$, $i = 1, 2$ (and no interaction with the thermal bath), thus the Hamiltonian of work corresponds to

$$\hat{H}_s(t) = \sum_{i=1}^{2} \left(-\frac{\epsilon_0 + A\cos(\omega t)}{2} \sigma_z^{(i)} \right) - \frac{J}{2}\left(\sigma_+^{(1)}\sigma_-^{(2)} + \sigma_-^{(1)}\sigma_+^{(2)}\right). \tag{A1}$$

Performing a basis change to the basis $\{|s_0\rangle, |e_+\rangle, |e_-\rangle, |s_1\rangle\}$, the Hamiltonian in Eq. (A1) becomes diagonal, allowing us to obtain the Floquet states as

$$\begin{aligned} \left|s_{\tilde{1}}^{\tilde{0}}(t)\right\rangle &= \sum_k e^{\pm i\omega k t} J_k\left(\frac{A}{\omega}\right) e^{-i\tilde{n}\omega t}\left|s_{\tilde{1}}^{\tilde{0}}\right\rangle, \\ |e_\pm(t)\rangle &= e^{-i\tilde{m}\omega t}|e_\pm\rangle, \end{aligned} \tag{A2}$$

with its corresponding quasienergies $\gamma_{\tilde{1}}^{\tilde{0}} = \mp\epsilon_0 - \tilde{n}\omega$ and $\gamma_\pm = \mp J/2 - \tilde{m}\omega$, with $\tilde{n}, \tilde{m} \in \mathbb{Z}$. $J_k(x)$ corresponds to the kth-order Bessel function.

In order to obtain the relaxation rate presented in Eq. (16), it will be useful to work in the Fourier extended basis. Making the corresponding expansion $|\alpha(t)\rangle = \sum_k |\alpha(k)\rangle e^{-ik\omega t}$, with $k \in \mathbb{Z}$ and α the state index, the corresponding expansion terms are

$$\begin{aligned} \left|\mathbf{s}_{\tilde{1}}^{\tilde{0}}(\tilde{n})\right\rangle &= \sum_k J_{\pm(\tilde{n}-k)}\left(\frac{A}{\omega}\right)\left|s_{\tilde{1}}^{\tilde{0}}, k\right\rangle, \\ |\mathbf{e}_\pm(\tilde{m})\rangle &= |e_\pm, \tilde{m}\rangle. \end{aligned} \tag{A3}$$

As long as Δ_i is small, the locations of the quasicrossings in the spectrum of quasienergies are replicas (in $\pm m\omega$) of the quasicrossings of the static spectrum. The resonance conditions $\gamma_\alpha - \gamma_\beta = n'\omega$ ($n' \in \mathbb{Z}$) are thus satisfied, respectively, $\epsilon_0 \pm J/2 \sim m'\omega$ (SE resonances), $2\epsilon_0 \sim m'\omega$ (SS resonances), and $J \sim m'\omega$ (EE resonances) with $m' \in \mathbb{Z}$. Considering this picture, we can work with an effective Hamiltonian 2×2 corresponding to a local system description when we are near a resonance condition. In this framework, Δ_i is treated as a perturbation, opening dynamical gaps between the two local states.

To be consistent with the results presented along this work, we are going to consider the effective Hamiltonian in the subspace $\mathcal{S} = \{|\mathbf{s}_0(\tilde{n})\rangle, |\mathbf{e}_+(\tilde{m})\rangle\}$ for the system dynamics near a SE resonance. In this case, the corresponding effective Hamiltonian (at first order) is

$$[\hat{H}_{\text{eff}}]_{\mathcal{S}} = \begin{pmatrix} \gamma_{0,\tilde{n}} & -\frac{\tilde{\Delta}_{\tilde{n}-\tilde{m}}}{2} \\ -\frac{\tilde{\Delta}_{\tilde{n}-\tilde{m}}}{2} & \gamma_{+,\tilde{m}} \end{pmatrix}, \tag{A4}$$

with $\gamma_{0,n} = -\epsilon_0 + \tilde{n}\omega$, $\gamma_{+,\tilde{m}} = -J/2 + \tilde{m}\omega$, and $\tilde{\Delta}_{\tilde{m}-\tilde{n}} = \sqrt{2}(\Delta_1 + \Delta_2)J_{\tilde{m}-\tilde{n}}(\frac{A}{\omega})$. Since we are close to the SE-resonance condition, the constraint $\gamma_0 - \gamma_+ = m'\omega$ must

be fulfilled, thus, $\gamma_{0,\tilde{n}} - \gamma_{+,\tilde{m}} = \gamma_0 - \gamma_+ - (\tilde{m} - \tilde{n})\omega = \gamma_0 - \gamma_+ - m'\omega = 0$ with $m' = \tilde{m} - \tilde{n}$, which brings us to the expression

$$[\hat{H}_{\rm eff}]_{\mathcal{S}} = \begin{pmatrix} \gamma_{0,\tilde{n}} & -\frac{\tilde{\Delta}_{-m'}}{2} \\ -\frac{\tilde{\Delta}_{-m'}}{2} & \gamma_{+,\tilde{n}+m'} \end{pmatrix}. \tag{A5}$$

Applying the second order of perturbation, we obtain

$$[\hat{H}_{1,\rm eff}]_{\mathcal{S}} = \begin{pmatrix} \gamma_{0,\tilde{n}} - \frac{1}{4}\sum_{l\neq m'} \frac{|\tilde{\Delta}_l|^2}{\gamma_{0,+}+l\omega} & -\frac{\tilde{\Delta}_{-m'}}{2} \\ -\frac{\tilde{\Delta}_{-m'}}{2} & \gamma_{+,\tilde{n}+m'} + \frac{1}{4}\sum_{l\neq m'} \frac{|\tilde{\Delta}_l|^2}{\gamma_{0,+}+l\omega} \end{pmatrix}. \tag{A6}$$

The solutions of Eq. (A6) are the expressions [38]

$$\begin{aligned} |a(\tilde{n})\rangle &= -\sin\left(\frac{\Theta_{m'}}{2}\right)|\mathbf{s}_0(\tilde{n})\rangle \\ &\quad - \mathrm{sign}(\tilde{\Delta}_{-m'})\cos\left(\frac{\Theta_{m'}}{2}\right)|\mathbf{e}_+(\tilde{n}+m')\rangle, \\ |b(\tilde{n}+m')\rangle &= \cos\left(\frac{\Theta_{m'}}{2}\right)|\mathbf{s}_0(\tilde{n})\rangle \\ &\quad - \mathrm{sign}(\tilde{\Delta}_{-m'})\sin\left(\frac{\Theta_{m'}}{2}\right)|\mathbf{e}_+(\tilde{n}+m')\rangle, \end{aligned} \tag{A7}$$

where

$$\Theta_{m'} = \arctan\left(\frac{|\tilde{\Delta}_{-m'}|}{-\gamma_{0,+} + m'\omega - \frac{1}{2}\sum_{l\neq -m'}\frac{|\tilde{\Delta}_l|^2}{\gamma_{0,+}+l\omega}}\right). \tag{A8}$$

Using the above solutions, we proceed to calculate A^n_{ab} the transition element matrix in the Floquet basis, for $\mathcal{A} = g(\sigma_z^{(1)} + \sigma_z^{(2)})$. The corresponding expression is

$$\begin{aligned} A^n_{ab} &= \sum_L \langle a(L)|\mathcal{A}|b(L+n)\rangle \\ &= -\sin\left(\frac{\Theta_n}{2}\right)\cos\left(\frac{\Theta_n}{2}\right)\sum_L \langle \mathbf{s}_0, L|\mathcal{A}|\mathbf{s}_0, L\rangle \\ &= -\frac{g}{2}\sin(\Theta_n) \\ &= \mp\frac{g}{2}\frac{\tan(\Theta_n)}{\sqrt{1+\tan^2(\Theta_n)}}, \end{aligned} \tag{A9}$$

replacing the expression of Θ_n [see Eq. (A8)], we obtain

$$A^n_{ab} = \mp\frac{g}{2}\frac{|\tilde{\Delta}_{-n}|}{\sqrt{\left(-\gamma_{ab} + n\omega - \frac{1}{2}\sum_{l\neq -n}\frac{|\Delta_l|^2}{\gamma_{ab}+l\omega}\right)^2 + |\tilde{\Delta}_{-n}|^2}}. \tag{A10}$$

In this way, the n-photon exchange terms $R_{aa,bb} = \sum_n g_{ab}|A^n_{ab}|^2$, from Eq. (6), can be computed as

$$\begin{aligned} R_{aa,bb} &= \frac{g^2}{4}\sum_n \frac{g^n_{ab}|\tilde{\Delta}_{-n}|^2}{\left(-\gamma_{ab} + n\omega - \frac{1}{2}\sum_{l\neq -n}\frac{|\Delta_l|^2}{\gamma_{ab}+l\omega}\right)^2 + |\tilde{\Delta}_{-n}|^2}, \\ R_{bb,aa} &\sim 0, \end{aligned} \tag{A11}$$

where we have considered the approximation $g^n_{ba} = e^{-\gamma^n_{ab}/k_bT_b} g^n_{ab} \to 0$ when $T_b \to 0$.

Finally, the relaxation rate Γ_r, presented in Eq. (16), can be expressed as

$$\begin{aligned} \Gamma_r &= \frac{g^2}{2}\sum_n \frac{g^n_{ab}|\tilde{\Delta}_{-n}|^2}{\left(-\gamma_{ab} + n\omega - \frac{1}{2}\sum_{l\neq -n}\frac{|\Delta_l|^2}{\gamma_{ab}+l\omega}\right)^2 + |\tilde{\Delta}_{-n}|^2} \\ &= \Gamma_r^{(0)} + \sum_{n\neq 0}\Gamma_r^{(n)}, \\ \Gamma_r^{(-n)} &= \frac{g^2}{2}\frac{g^n_{ab}|\tilde{\Delta}_{-n}|^2}{\left(\gamma_{ab} - n\omega + \frac{1}{2}\sum_{l\neq -n}\frac{|\Delta_l|^2}{\gamma_{ab}+l\omega}\right)^2 + |\tilde{\Delta}_{-n}|^2}. \end{aligned} \tag{A12}$$

As it is discussed in the main body of the paper, we are interested in the relaxation rates $\Gamma_r^{(0)}$ and $\Gamma_r^{(-m')}$, with $n = m'$ corresponding to the chosen example, which satisfy the constraint $\gamma_0 - \gamma_+ = -\epsilon_0 + J/2 = m'\omega$. Using Eq. (A12), we obtain

$$\begin{aligned} \Gamma_r^{(0)} &= \frac{g^2}{2}\frac{g^0_{ab}|\tilde{\Delta}_0|^2}{\left(\gamma_{ab} + \frac{1}{2}\sum_{l\neq 0}\frac{|\Delta_l|^2}{\gamma_{ab}+l\omega}\right)^2 + |\tilde{\Delta}_0|^2}, \\ \Gamma_r^{(-m')} &= \frac{g^2}{2}\frac{g^{-m'}_{ab}|\tilde{\Delta}_{-m'}|^2}{\left(\gamma_{ab} - m'\omega + \frac{1}{2}\sum_{l\neq m'}\frac{|\Delta_l|^2}{\gamma_{ab}+l\omega}\right)^2 + |\tilde{\Delta}_{-m'}|^2}, \end{aligned} \tag{A13}$$

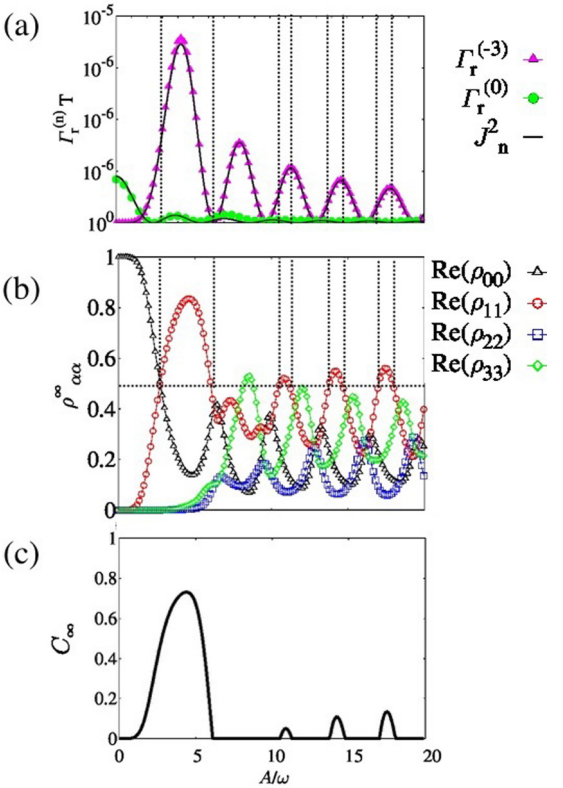

FIG. 5. Plot of $\Gamma_r^{(n)}$ terms that contribute to the relaxation rate (a), population of the Floquet states $\rho^\infty_{\alpha\alpha}$ (b), and concurrence C_∞ (c), as a function of A/ω. All the cases correspond to the fixed value $\epsilon_0/\omega = 4.1$. The other parameters are the same as presented in Fig. 1. The black lines in (a) correspond to the approximation $\Gamma_r^{(n)} \propto J_n^2(A/\omega)$.

replacing with the corresponding expression for $\tilde{\Delta}_n$

$$\Gamma_r^{(0)} = \frac{g^2/2g_{ab}^0 2(\Delta_1+\Delta_2)^2 J_0\left(\frac{A}{\omega}\right)^2}{\left(\gamma_{ab}+\frac{1}{2}\sum_{l\neq 0}\frac{|\Delta_l|^2}{\gamma_{ab}+l\omega}\right)^2+2(\Delta_1+\Delta_2)^2 J_0\left(\frac{A}{\omega}\right)^2},$$
$$\Gamma_r^{(-m')} = \frac{g^2/2g_{ab}^{-m'} 2(\Delta_1+\Delta_2)^2 J_{-m'}\left(\frac{A}{\omega}\right)^2}{\left(\gamma_{ab}-m'\omega+\frac{1}{2}\sum_{l\neq m'}\frac{|\Delta_l|^2}{\gamma_{ab}+l\omega}\right)^2+2(\Delta_1+\Delta_2)^2 J_{-m'}\left(\frac{A}{\omega}\right)^2}. \tag{A14}$$

From Eq. (A14) it follows that the dominant dependence with A/ω of the relaxation rates is $\Gamma_r^{(0)} \propto J_0^2(\frac{A}{\omega})$ and $\Gamma_r^{(-m')} \propto J_{-m'}^2(\frac{A}{\omega})$. This Bessel function dependence can be better observed if we extend the numerical calculation of the $\Gamma_r^{(n)}$ for values of A/ω larger than the case shown in the main body of the paper. As an example, we choose the off-resonant case $\epsilon_0/\omega = 4.1$, that is close to the $(m = 3)$-photon resonance at $\epsilon_0/\omega = 4.25$. We plot in Fig. 5 as a function of A the relaxation rates $\Gamma_r^{(n)}$, the population of the states in the steady state $\rho_{\alpha\alpha}^{\infty}$, and the concurrence C_∞. As it is shown in Fig. 5(a) the approximation $\Gamma_r^{(n)} \propto J_n^2(A/\omega)$ agrees very well with the values of $\Gamma_r^{(n)}$ obtained numerically from the direct evaluation of Eq. (16). Furthermore, in Fig. 5(b) we see that while the amplitude satisfies $A \lesssim |\epsilon_0|$, the population transfer only takes place between the states $|E_0\rangle$ (black triangles) and $|E_1\rangle$ (red circles) [see Fig. 1(d)]. But, when the amplitude increases, more avoided crossings are reached in the range $[\epsilon_0 - A, \epsilon_0 + A]$ spanned by the driving, allowing to populate the states $|E_2\rangle$ and $|E_3\rangle$. In this latter situation, the two-level approximation loses validity for $A \gg |\epsilon_0|$. For amplitudes A within the two-level regime, we see that there is population inversion whenever the $\Gamma_r^{(-3)}$ term is the largest one and $C_\infty \neq 0$. It is interesting to point out that for large A, where the calculation of the plotted $\Gamma_r^{(n)}$ is no longer valid, there is a finite value of concurrence whenever the population of the first excited state is the largest. Thus, even when the dynamics is more complex, involving all the four states, the qualitative picture of entanglement generation due to population inversion is still correct.

[1] B. Kraus, H. P. Büchler, S. Diehl, A. Kantian, A. Micheli, and P. Zoller, Phys. Rev. A **78**, 042307 (2008).

[2] F. Verstraete, M. M. Wolf, and J. I. Cirac, Nat. Phys. **5**, 633 (2009).

[3] F. Reiter, L. Tornberg, G. Johansson, and A. S. Sørensen, Phys. Rev. A **88**, 032317 (2013).

[4] F. Tacchino, A. Auffèves, M. F. Santos, and D. Gerace, Phys. Rev. Lett. **120**, 063604 (2018).

[5] J. T. Barreiro, M. Müller, P. Schindler, D. Nigg, T. Monz, M. Chwalla, M. Hennrich, C. F. Roos, P. Zoller, and R. Blatt, Nature (London) **470**, 486 (2011).

[6] Y. Lin, J. P. Gaebler, F. Reiter, T. R. Tan, R. Bowler, A. S. Sørensen, D. Leibfried, and D. J. Wineland, Nature (London) **504**, 415 (2013).

[7] D. Kienzler, H.-Y. Lo, B. Keitch, L. de Clercq, F. Leupold, F. Lindenfelser, M. Marinelli, V. Negnevitsky, and J. P. Home, Science **347**, 53 (2015).

[8] H. Krauter, C. A. Muschik, K. Jensen, W. Wasilewski, J. M. Petersen, J. I. Cirac, and E. S. Polzik, Phys. Rev. Lett. **107**, 080503 (2011).

[9] S. Shankar, M. Hatridge, Z. Leghtas, K. M. Sliwa, A. Narla, U. Vool, S. M. Girvin, L. Frunzio, M. Mirrahimi, and M. H. Devoret, Nature (London) **504**, 419 (2013).

[10] Z. Leghtas, U. Vool, S. Shankar, M. Hatridge, S. M. Girvin, M. H. Devoret, and M. Mirrahimi, Phys. Rev. A **88**, 023849 (2013).

[11] M. E. Kimchi-Schwartz, L. Martin, E. Flurin, C. Aron, M. Kulkarni, H. E. Tureci, and I. Siddiqi, Phys. Rev. Lett. **116**, 240503 (2016).

[12] C. M. Quintana, K. D. Petersson, L. W. McFaul, S. J. Srinivasan, A. A. Houck, and J. R. Petta, Phys. Rev. Lett. **110**, 173603 (2013).

[13] P. Campagne-Ibarcq, E. Zalys-Geller, A. Narla, S. Shankar, P. Reinhold, L. Burkhart, C. Axline, W. Pfaff, L. Frunzio, R. J. Schoelkopf, and M. H. Devoret, Phys. Rev. Lett. **120**, 200501 (2018).

[14] L. DiCarlo, J. M. Chow, J. M. Gambetta, L. S. Bishop, B. R. Johnson, D. I. Schuster, J. Majer, A. Blais, L. Frunzio, S. M. Girvin, and R. J. Schoelkopf, Nature (London) **460**, 240 (2009).

[15] D. Ristè, M. Dukalski, C. A. Watson, G. de Lange, M. J. Tiggelman, Y. M. Blanter, K. W. Lehnert, R. N. Schouten, and L. DiCarlo, Nature (London) **502**, 350 (2013).

[16] N. Roch, M. E. Schwartz, F. Motzoi, C. Macklin, R. Vijay, A. W. Eddins, A. N. Korotkov, K. B. Whaley, M. Sarovar, and I. Siddiqi, Phys. Rev. Lett. **112**, 170501 (2014).

[17] A. Chantasri, M. E. Kimchi-Schwartz, N. Roch, I. Siddiqi, and A. N. Jordan, Phys. Rev. X **6**, 041052 (2016).

[18] Y. Liu, S. Shankar, N. Ofek, M. Hatridge, A. Narla, K. M. Sliwa, L. Frunzio, R. J. Schoelkopf, and M. H. Devoret, Phys. Rev. X **6**, 011022 (2016).

[19] F. Grossmann, T. Dittrich, P. Jung, and P. Hänggi, Phys. Rev. Lett. **67**, 516 (1991).

[20] I. Bloch, J. Dalibard, and S. Nascimbène, Nat. Phys. **8**, 267 (2012).

[21] D. Gagnon, F. Fillion-Gourdeau, J. Dumont, C. Lefebvre, and S. MacLean, Phys. Rev. Lett. **119**, 053203 (2017).

[22] W. D. Oliver, Y. Yu, J. C. Lee, K. K. Berggren, L. S. Levitov, and T. P. Orlando, Science **310**, 1653 (2005).

[23] M. Sillanpää, T. Lehtinen, A. Paila, Y. Makhlin, and P. Hakonen, Phys. Rev. Lett. **96**, 187002 (2006).

[24] D. M. Berns, W. D. Oliver, S. O. Valenzuela, A. V. Shytov, K. K. Berggren, L. S. Levitov, and T. P. Orlando, Phys. Rev. Lett. **97**, 150502 (2006).

[25] M. S. Rudner, A. V. Shytov, L. S. Levitov, D. M. Berns, W. D. Oliver, S. O. Valenzuela, and T. P. Orlando, Phys. Rev. Lett. **101**, 190502 (2008).

[26] A. Izmalkov, S. H. W. van der Ploeg, S. N. Shevchenko, M. Grajcar, E. Il'ichev, U. Hübner, A. N. Omelyanchouk, and H.-G. Meyer, Phys. Rev. Lett. **101**, 017003 (2008).

[27] S. Shevchenko, S. Ashhab, and F. Nori, Phys. Rep. **492**, 1 (2010).

[28] C. M. Wilson, G. Johansson, T. Duty, F. Persson, M. Sandberg, and P. Delsing, Phys. Rev. B **81**, 024520 (2010).

[29] E. Dupont-Ferrier, B. Roche, B. Voisin, X. Jehl, R. Wacquez, M. Vinet, M. Sanquer, and S. De Franceschi, Phys. Rev. Lett. **110**, 136802 (2013).

[30] F. Forster, G. Petersen, S. Manus, P. Hänggi, D. Schuh, W. Wegscheider, S. Kohler, and S. Ludwig, Phys. Rev. Lett. **112**, 116803 (2014).

[31] P. Neilinger, S. N. Shevchenko, J. Bogár, M. Rehák, G. Oelsner, D. S. Karpov, U. Hübner, O. Astafiev, M. Grajcar, and E. Il'ichev, Phys. Rev. B **94**, 094519 (2016).

[32] T. M. Stace, A. C. Doherty, and S. D. Barrett, Phys. Rev. Lett. **95**, 106801 (2005).

[33] T. M. Stace, A. C. Doherty, and D. J. Reilly, Phys. Rev. Lett. **111**, 180602 (2013).

[34] A. Ferrón, D. Domínguez, and M. J. Sánchez, Phys. Rev. Lett. **109**, 237005 (2012).

[35] A. Ferrón, D. Domínguez, and M. J. Sánchez, Phys. Rev. B **93**, 064521 (2016).

[36] J. H. Shirley, Phys. Rev. **138**, B979 (1965).

[37] M. Grifoni and P. Hänggi, Phys. Rep. **304**, 229 (1998).

[38] J. Hausinger and M. Grifoni, Phys. Rev. A **81**, 022117 (2010).

[39] A. Ferrón, D. Domínguez, and M. J. Sánchez, Phys. Rev. B **82**, 134522 (2010).

[40] S. Sauer, F. Mintert, C. Gneiting, and A. Buchleitner, J. Phys. B: At. Mol. Opt. Phys. **45**, 154011 (2012).

[41] A. L. Gramajo, D. Domínguez, and M. J. Sánchez, Eur. Phys. J. B **90**, 255 (2017).

[42] We obtain similar results as reported here when an interaction term $\sigma_z^{(1)}\sigma_z^{(2)}$ is considered instead of $\sigma_+^{(1)}\sigma_-^{(2)} + \sigma_-^{(1)}\sigma_+^{(2)}$.

[43] A. J. Berkley, H. Xu, R. C. Ramos, M. A. Gubrud, F. W. Strauch, P. R. Johnson, J. R. Anderson, A. J. Dragt, C. J. Lobb, and F. C. Wellstood, Science **300**, 1548 (2003).

[44] A. Izmalkov, M. Grajcar, E. Il'ichev, T. Wagner, H.-G. Meyer, A. Y. Smirnov, M. H. S. Amin, A. Maassen van den Brink, and A. M. Zagoskin, Phys. Rev. Lett. **93**, 037003 (2004).

[45] J. B. Majer, F. G. Paauw, A. C. J. ter Haar, C. J. P. M. Harmans, and J. E. Mooij, Phys. Rev. Lett. **94**, 090501 (2005).

[46] Y.-x. Liu, L. F. Wei, J. S. Tsai, and F. Nori, Phys. Rev. Lett. **96**, 067003 (2006).

[47] J. Zhang, Y.-x. Liu, C.-W. Li, T.-J. Tarn, and F. Nori, Phys. Rev. A **79**, 052308 (2009).

[48] S. J. Weber, G. O. Samach, D. Hover, S. Gustavsson, D. K. Kim, A. Melville, D. Rosenberg, A. P. Sears, F. Yan, J. L. Yoder, W. D. Oliver, and A. J. Kerman, Phys. Rev. Appl. **8**, 014004 (2017).

[49] S. N. Shevchenko, S. H. W. van der Ploeg, M. Grajcar, E. Il'ichev, A. N. Omelyanchouk, and H.-G. Meyer, Phys. Rev. B **78**, 174527 (2008).

[50] E. Il'ichev, S. N. Shevchenko, S. H. W. van der Ploeg, M. Grajcar, E. A. Temchenko, A. N. Omelyanchouk, and H.-G. Meyer, Phys. Rev. B **81**, 012506 (2010).

[51] A. M. Satanin, M. V. Denisenko, S. Ashhab, and F. Nori, Phys. Rev. B **85**, 184524 (2012).

[52] E. A. Temchenko, S. N. Shevchenko, and A. N. Omelyanchouk, Phys. Rev. B **83**, 144507 (2011).

[53] S. Kohler, T. Dittrich, and P. Hänggi, Phys. Rev. E **55**, 300 (1997).

[54] S. Kohler, R. Utermann, P. Hänggi, and T. Dittrich, Phys. Rev. E **58**, 7219 (1998).

[55] D. W. Hone, R. Ketzmerick, and W. Kohn, Phys. Rev. E **79**, 051129 (2009).

[56] S. Gasparinetti, P. Solinas, S. Pugnetti, R. Fazio, and J. P. Pekola, Phys. Rev. Lett. **110**, 150403 (2013).

[57] V. Gramich, S. Gasparinetti, P. Solinas, and J. Ankerhold, Phys. Rev. Lett. **113**, 027001 (2014).

[58] W. K. Wootters, Phys. Rev. Lett. **80**, 2245 (1998).

[59] Y. Nakamura, Y. A. Pashkin, and J. S. Tsai, Phys. Rev. Lett. **87**, 246601 (2001).

[60] H.-P. Breuer, W. Huber, and F. Petruccione, Phys. Rev. E **61**, 4883 (2000).

[61] R. Blümel, A. Buchleitner, R. Graham, L. Sirko, U. Smilansky, and H. Walther, Phys. Rev. A **44**, 4521 (1991).

[62] K. Szczygielski, J. Math. Phys. **55**, 083506 (2014).